Journal of Colloid and Interface Science 555 (2019) 569–582

Contents lists available at ScienceDirect

Journal of Colloid and Interface Science

journal homepage: www.elsevier.com/locate/jcis

Regular Article

Ultrahigh-flux (>190,000 $L \cdot m^{-2}h^{-1}$) separation of oil and water by a robust and durable $Cu(OH)_2$ nanoneedles mesh with inverse wettability

Ruixia Yuan [a,b], Jincheng Liu [a], Zhijun Li [a], Yanguang Chen [a], Zhaohui Wang [c,d,*], Zhanjian Liu [a], Guolin Jing [a], Yanji Zhu [a], Huaiyuan Wang [a,*]

[a] College of Chemistry and Chemical Engineering, Northeast Petroleum University, Daqing, 163318, China
[b] Guangzhou Key Laboratory of Environmental Catalysis and Pollution Control, School of Environmental Science and Engineering, Institute of Environmental Health and Pollution Control, Guangdong University of Technology, Guangzhou 510006, China
[c] Shanghai Key Laboratory of Urbanization and Ecological Restoration, School of Ecological and Environmental Sciences, East China Normal University, Shanghai 200241, China
[d] Institute of Eco-Chongming (IEC), Shanghai 200062, China

GRAPHICAL ABSTRACT

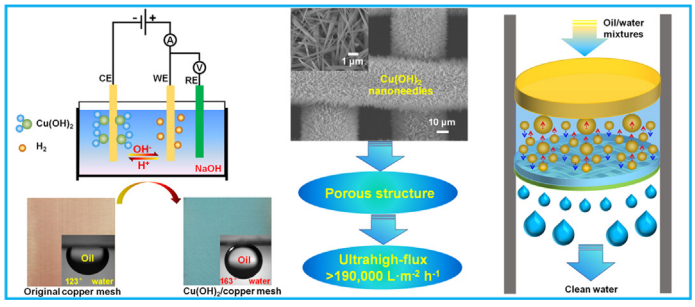

ARTICLE INFO

Article history:
Received 3 July 2019
Revised 1 August 2019
Accepted 3 August 2019
Available online 5 August 2019

Keywords:
Underwater superoleophobicity
Superhydrophilicity
Oil/water separation
Permeating flux
Chemical stability

ABSTRACT

Single-stage oil/water separation membranes usually suffer from weak chemical stability, susceptible mechanical damage and relatively low permeating flux, and the sophisticated preparation processes also limit their massive utilization. In this work, $Cu(OH)_2$ nanoneedles coated copper mesh (CM) is prepared by simple and eco-friendly anodic oxidation at a current density of 4 mA/cm^2 for 6 min, which is the most efficient route reported so far. The mesh exhibits outstanding superhydrophilicity and underwater superoleophobicity towards various oils with contact angles up to 164.9°, achieving superior oil/water separation efficiency of above 99.5% and ultrahigh permeating flux of 191 160 $L \cdot m^{-2}h^{-1}$ solely driven by gravity. Impressively, the $Cu(OH)_2$/CM demonstrates excellent chemical stability and anti-fouling performance when exposed to acidic and strongly alkaline solutions, saturated NaCl solution and various organic solvents. High durability to withstand mechanical challenges, e.g. high-power sonication and sand abrasion, is experimentally confirmed owing to strong cohesional strength of $Cu(OH)_2$ nanoneedles on CM surface. Importantly, the $Cu(OH)_2$/CM exhibits favorable long-term recyclability with stable microstructure morphologies even after 50 cycles. These distinct advantages endow the $Cu(OH)_2$/CM to be an ideal candidate to efficiently separate oil pollutants from water. The oil/water separation mechanisms are proposed based on the concept of intrusion pressure.

1. Introduction

The frequent crude oil spillage and increasing discharge of industrial oily effluent have posed great threaten to the environ-

* Corresponding authors.
E-mail addresses: zhwang@des.ecnu.edu.cn (Z. Wang), wanghyjiji@163.com (H. Wang).

https://doi.org/10.1016/j.jcis.2019.08.011
0021-9797/

mental and ecological safety, rendering the oil/water separation become a worldwide subject [1,2]. Traditional approaches, including air flotation, oil absorption, centrifugation, flocculation and coagulation, usually suffer from low separation efficiency and selectivity, high operation cost and energy consumption [3–5]. Therefore, it is urgently demanded to exploit advanced technologies for rapid and effective oily wastewater remediation from both scientific and practical aspects [6–8].

Recently, functional membranes with special surface wettability towards water and oil have attracted considerable attention owing to the advantages of flexible usability and high single-stage separation efficiency [9–11]. However, the superhydrophobic and superoleophilic membranes are vulnerable to be fouled and even plugged by the adhered oil, resulting in a significant reduction of separation efficiency [6,12]. Moreover, as most of oils have lower density than water, the sandwiched water phase between the oil and membrane surface could retard the infiltration of oil phase, resulting in rapid decline in the permeating flux [13,14].

The particular oil-repellent and anti-fouling phenomenon of fish scales in oil contaminated ocean has triggered increasing research interest [15–17]. Inspired by this, constructing superhydrophilic and underwater superoleophobic interface is assumed to provide an alternative route to overcome the aforementioned issues [16,18,19]. As water is readily trapped into the rough microstructures of superhydrophilic membranes, a thin water layer can be formed to promote the continuous water filtration and provide a strong repulsive force towards oils. Accordingly, the oil penetration through the membrane pores and the fouling of the membrane during usage are effectively depressed. Thus, high oil/water separation efficiency can be achieved [20,21]. The water flux is a critical index to evaluate the permeability of the separation membranes [22]. The permission flux is described by the classical fluid theory of Hagen-Poiseuille (Eq. (1)) [23]:

$$J = \frac{\varepsilon \pi r_p^2 \Delta p}{8 \mu L} \tag{1}$$

In which J is the permeating flux of the liquid, ε is the porosity, r_p is the effective pore radius, μ is the viscosity of the liquid and L is the thickness of the membrane.

So far, intrinsic hydrophilic materials, such as metal oxides and hydroxides [24,25], graphene oxide [26], zeolites [27], cellulose [28] and hydrogels [29] have already been decorated on various substrates in pursuit of desirable superhydrophilicity and underwater superoleophobicity. However, bottleneck of low permeating flux still remains for the organic materials (e.g. sponges, foams and filtration fabrics), because of their initial defects of relatively small pore size [30,31]. Further improving the porosity of organic polymer composite membranes are also restricted by their highly compact structures and functional additives, which underpin their mechanical strength and selective wettability [32].

In theory, metal meshes with 3D interconnected networks and high porous structures allow a higher permeating flux for sufficient oil/water separation [33]. Moreover, the favorable mechanical robustness and easy reuse without squeezing also ensure the metal meshes more potential for long-term usage. Various strategies, including hydrothermal [33], chemical etching [22], chemical vapor deposition [34] and electrochemical method [19], have been successfully applied to create hydrophilic structures on metal mesh. For example, Lai et al. [22] prepared $Cu(OH)_2$-coated copper mesh (CM) by immersion in $HS(CH_2)_{11}OH$ for 12 h. The observed superhydrophilicity and underwater superoleophobicity as well as the resultant high oil/water separation efficiency (>99.8%) can be attributed to the cooperative effect of the nanostructures and hydrophilic hydroxyl groups. You et al. [19] developed coral-like Zn-ZnO nanostructures on CM at a voltage of 8 V for 2 h. Superhydrophilic and high underwater oil-repellency with oil contact angle (OCA) of above 151° were demonstrated and more than 99.0% oils can be removed from water. Zhu et al. [35] employed electrochemical oxidation method to obtain hierarchical nanoneedles-like Cu $(OH)_2$ coated stainless steel fiber felts (SSFF) with underwater superoleophobic and low-adhesive properties. The SSFF required to be pretreated by high vacuum sputtering of gold layer and afterwards electrodeposition of copper nanoparticles. Liu et al. [36] fabricated polyaniline-coated CM by electrochemical polymerization using 0.1 M aniline as an electrolyte, achieving effective oil-water separation. However, most of the reported approaches still have limitations for mass production because of the time-consuming and complicated pretreatment processes, usage of high toxic materials or expensive facilities [6,17]. Furthermore, rapid decay in separation capability due to poor susceptible mechanical damage and weak chemical stability are usually another obstacles for widespread utilization.

Herein, in this study, we first exploit one-step anodic oxidation route to design $Cu(OH)_2$ nanoneedles on copper mesh aiming for superior superhydrophilic and underwater superoleophobic capability. This technology is fairly facile, environmentally benign and highly efficient for mass production. By optimizing the current density and reaction duration, highly efficient oil/water separation is realized. In addition, the as-prepared $Cu(OH)_2$/CM seems a perfect combination of great reusability, high permeation flux, heat resistance, mechanical and chemical stability, which make the mesh very promising toward durable oil/water separation under severe conditions.

2. Experimental section

2.1. Materials

Commercial copper meshes were purchased from Hengshui Wire Mesh Products Co. Ltd. (China). NaOH, HCl (36 wt%), NaCl, acetone, dichloromethane (DCM), hexane, *N,N*-dimethylformamide (DMF), ethanol (EtOH), ethyl acetate (EtOAc) and methanol (MeOH) were provided by Aladdin Reagent Co. Ltd. (China). Gasoline, kerosene and diesel were supplied by local gas station.

2.2. Preparation of $Cu(OH)_2$ nanoneedles coated CM

The copper mesh was successively degreased under ultrasonication in acetone, ethanol and deionized water for 20 min, followed by drying in air. Afterward, the electrochemical oxidation was conducted at ambient temperature with a three-electrode electrochemical cell, using 1 M NaOH solution as an electrolyte (Fig. 1a). The pre-treated meshes were used as both working electrode (anode) and counter electrode (cathode), and saturated calomel electrode as reference electrode (RE). Finally, the coated CM was rinsed with deionized water for several times and dried in air for subsequent use.

2.3. Characterization

The morphological structures of the samples were observed with a Zeiss SIGMA field emission scanning electron microscope (SEM) at 10 kV. The chemical components of the formed $Cu(OH)_2$ on CM was examined with Oxford X-Max type energy dispersive spectrometer (EDS) and X-ray diffraction (XRD) (D/max 2200). The contact angles of water/oil for the mesh were measured using Contact Angle Meter (JGW-360A). Thermogravimetric (TG) was conducted using thermogravimetric analyzers (STA73000) at a heating rate of 10 °C/min under air atmosphere.

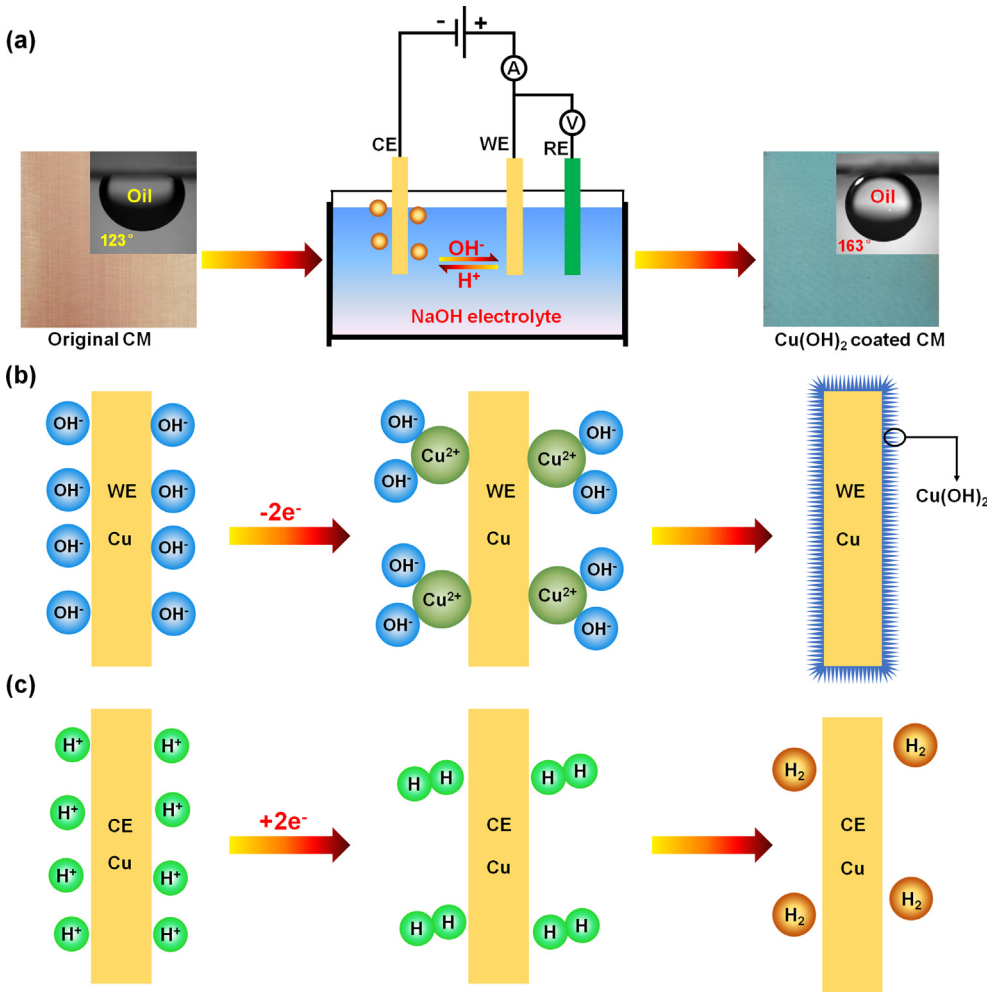

Fig. 1. Schematic of (a) preparation process of the $Cu(OH)_2$/CM, the electrochemical reactions at (b) working electrode (WE) and (c) counter electrode (CE).

2.4. Oil/water separation

The oil/water separation was performed as follows: the coated mesh was first completely pre-wetted by deionized water and then firmly fixed between two glass tubes in 20 mm diameter for oil/water separation. The oily liquids were colored by Oil Red O for better visual discrimination, followed by mixing with water (V_{oil}: V_{water} = 1:4). In general, 100 mL oil/water mixture was delivered into the glass tube assisted by a peristaltic pump and separated by the $Cu(OH)_2$/CM under the gravity drive. The separation efficiency (SE) was calculated according to the following equation:

$$SE\ (\%) = \frac{m_1}{m_0} \times 100\% \quad (2)$$

where m_0 is the weight of pristine oil in the mixture before separation, and m_1 represents the weight of collected oil after separation.

3. Results and discussion

3.1. Morphology and chemical composition

The pristine mesh composed of intertwined metal wires has relatively smooth texture with pore diameter of approximately 40 μm (Fig. 2a1). After electrochemical oxidation, the external surface of the mesh frame was densely and uniformly covered by Cu $(OH)_2$ nanoneedles (Fig. 2b1 and c). The resultant rough hierarchical architecture is essential for the required opposite wettability at two sides for oil/water separation. As the nanoneedles with length of about 5 μm grew vertically along the mesh walls and interconnected with each other, the effective pore size of the coated mesh greatly shrinked to circa 20 μm. This is benefit for the entrapment of oily droplet on the mesh surface.

Both element mappings and EDS spectrum of the raw copper mesh indicate the high purity of Cu (99% in atomic percentage) with trace oxygen element (1%) (Fig. 2a2, a3 and d). As for the coated sample, the much brighter areas of the oxygen mapping image suggest a higher content of oxygen (66%) (Fig. 2b2, b3 and d). The atomic number ratio of O to Cu is 1.94:1, close to the theoretical value of $Cu(OH)_2$. Apparently, both Cu and O are evenly distributed across the mesh wires, confirming the growth uniformity of the $Cu(OH)_2$ nanoneedles.

The XRD patterns of the original and coated meshes are displayed in Fig. 2e. The diffraction peaks at 42.66°, 50.04° and 74.46° in both spectra can be ascribed to the reflections from (1 1 1), (2 0 0) and (2 2 0) planes of metallic Cu (JCPDS Card No. 04-0836), respectively [25]. For the coated CM, three new characteristic peaks appear at 21.6°, 23.74° and 34.12°, which can be indexed as the (0 2 0), (0 2 1) and (0 0 2) planes of orthorhombic $Cu(OH)_2$ (JCPDS Card No. 80-0656) [35]. No evident peaks from other phase in the patterns can be observed, implying the pure crystalline structure of $Cu(OH)_2$.

Accordingly, the electrodeposition mechanism of $Cu(OH)_2$ nanoneedles on CM are expressed by Eqs. (3)–(5) [35]. Cu^{2+} ions were transformed from metallic Cu at anode by losing two

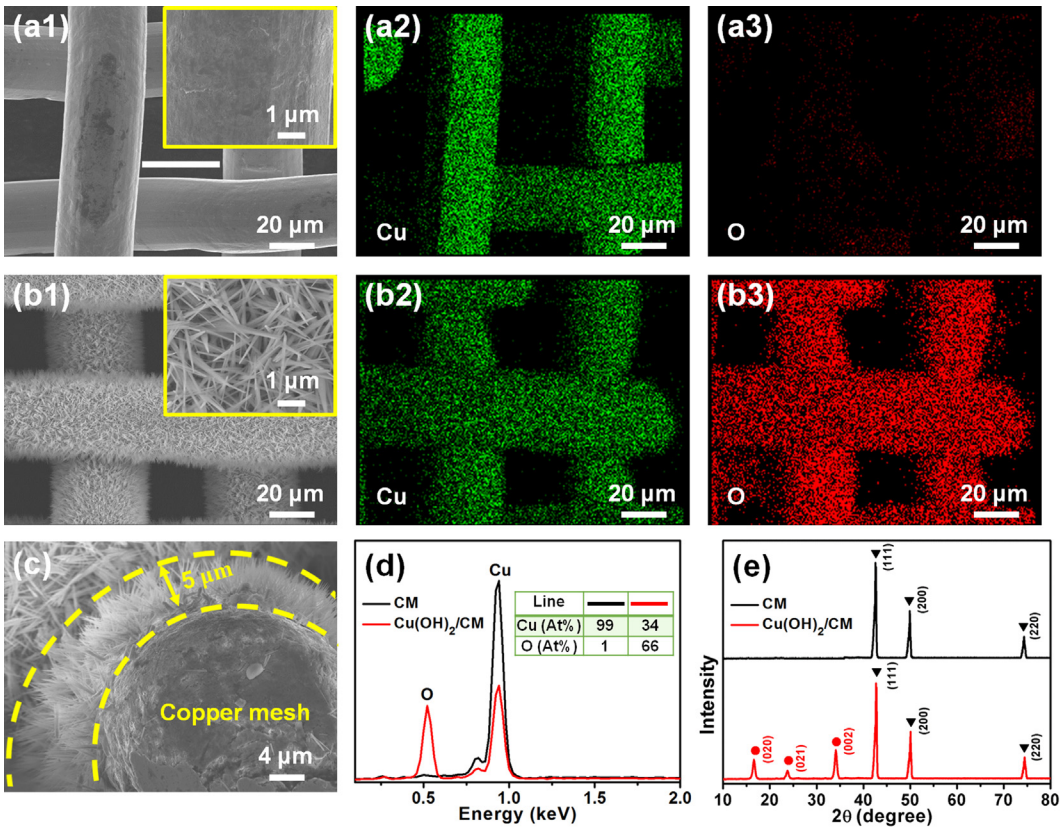

Fig. 2. Typical SEM images of (a1) original copper mesh and (b1) $Cu(OH)_2$/CM at low and (inset) high magnifications, (c) cross-section of the $Cu(OH)_2$/CM. Element mapping of Cu and O of (a2, a3) original copper mesh and (b2, b3) $Cu(OH)_2$/CM. (d) EDS and (e) XRD spectra of the original copper mesh and $Cu(OH)_2$/CM.

electrons, and $Cu(OH)_2$ was then generated on the CM surface via precipitation reaction between Cu^{2+} and the hydrolyzed OH^- [37]. Afterwards, the compact seed layer gradually grew to form nanoneedles morphology with prolonging reaction time (Fig. 1b). Simultaneously, the free H^+ captured electrons to produce H_2 at the cathode, and the resultant alkaline region nearby could further promote the deposition process of $Cu(OH)_2$ (Fig. 1c). After electrochemical treatment, the yellow CM completely turned into blue (Fig. 1a), indicating the dense distribution of $Cu(OH)_2$ nanoneedles on CM surface.

$$\text{Anode: } Cu(s) \rightarrow Cu^{2+}(s) + 2e^- \quad (3)$$

$$Cu^{2+}(s)+2OH^-(aq) \rightarrow Cu(OH)_2(s) \quad (4)$$

$$\text{Cathode: } 2H^+(aq)+2e^- \rightarrow H_2(g) \quad (5)$$

3.2. Wetting properties

The raw mesh exhibits weak hydrophobicity (WCA = 118.9°) in air and oleophobicity (OCA = 103.3°) in water (Fig. 3a and b). Nevertheless, the $Cu(OH)_2$/CM possesses superhydrophilic surface (WCA = 0°), which offers strong repulsive force to kerosene droplet as a consequence of their large difference in polarity. High underwater superoleophobicity with OCA of 164.9° can be evidenced by the approximate spherical shape of kerosene drop in water (Fig. 3c and d). In addition, the $Cu(OH)_2$/CM also has outstanding rejection capability towards other oily liquids (i.e. gasoline, diesel, hexane, bean oil and dichloromethane (DCM)) with high CAs ranging from 156.5° to 164.9° (Fig. 3e). The varying CAs may be ascribed to the different surface tension and viscosity of the oils [37].

Moreover, the underwater sliding angles (SAs) of $Cu(OH)_2$/CM towards various oils ranged from 1.0° to 1.8° (Fig. S1), and the DCM droplet could easily slide from a slightly titled surface of the mesh (Fig. S2). The oil adhesive behavior of the mesh was further investigated using a syringe needle according to the previous studies [38,39]. As seen in Fig. S3, the oil droplet was initially squeezed against the mesh surface under the preloading force. As the external pressure was gradually released, the droplet could maintain its spherical shape with no noticeable deformation, revealing the extremely low adhesion of oils on the membrane surface [40,41].

It is reported that the wettability of the solid surface greatly depends on its micro/nanostructure and chemical composition [42]. The special surface wettability of $Cu(OH)_2$/CM could be attributed to the cooperative effect of hydrophilic polar hydroxyl groups from $Cu(OH)_2$ nanoneedles and the binary nano/micro-scaled structures (Fig. 3f) [43,44]. The hydroxyl groups with extremely high surface energy are assumed to endow the mesh with the superhydrophilic surface and high water capture percentage [45]. The water-favoring ability of the mesh was estimated by measuring water capture percentage (WCP) according to Eq. (6) [25].

$$WCP(\%) = \frac{W_b - W_a}{W_a} \times 100\% \quad (6)$$

where W_a represents the original mass of the mesh, W_b stands for the mass of the mesh after immersed in water and then quickly taken out from water.

It is found that the WCP value of the mesh was dramatically improved from 5.6% to 53.3% after in situ growth of $Cu(OH)_2$ nanoneedles. Consequently, a huge amount of water would be efficiently trapped into the hierarchically structured porosity. A stable water cushion on the completely wetted CM surface can be thereby

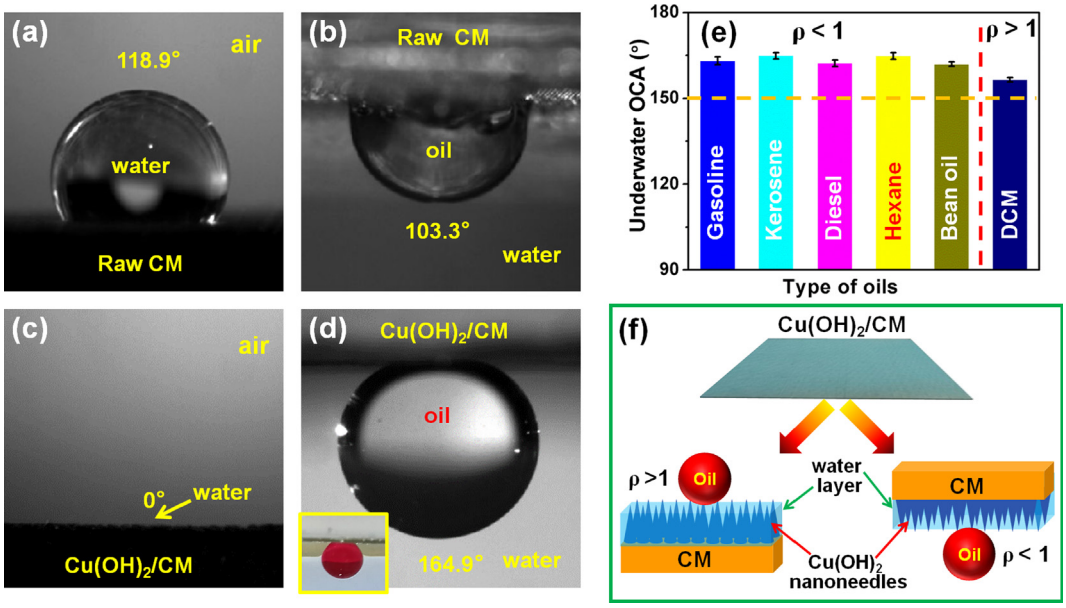

Fig. 3. Wetting behaviors of (a,b) original copper mesh and (c,d) $Cu(OH)_2$/CM. (e) Underwater OCA of $Cu(OH)_2$/CM towards a series of oils with density (ρ) higher or lower than that of H_2O (1 g/mL). Inset of (d) is the kerosene droplet (f) below the surface of $Cu(OH)_2$/CM in water. Schematic illustration of oil wetting on the hierarchical surface of $Cu(OH)_2$/CM in water.

formed, which offers a strong repelling force to the oily liquids [46].

When a three-phase interface system of oil-water-solid is formed on the $Cu(OH)_2$/CM surface, high underwater OCA can be described by the Cassie-Baxter model (Eq. (7)) [19,47]:

$$\cos\theta = f\cos\theta_1 + (1-f) \tag{7}$$

where θ and θ_1 represent the underwater OCA on the surface of rough coated mesh and pristine mesh, respectively, and f is defined as the area fraction of the solid surface in contact with oily droplet.

Theoretically, the contact chance of oil droplet with the mesh surface is very low at small area fraction, hence leading to a high underwater OCA. In our work, based on the CAs towards kerosene on the original mesh (~103.3°) and coated mesh (~164.9°), the area fraction f is estimated to be 0.087. This means only 8.7% of the area arising from oil/mesh contact interface. Thus, the predominant hydrophilicity and underwater superoleophobic ability can be achieved for the $Cu(OH)_2$/CM, which may endow a remarkable oil/water separation performance.

3.3. Optimization of the electrochemical conditions for oil/water separation

3.3.1. Influence of anodic oxidation time

The morphology evolution of $Cu(OH)_2$ nanoneedles as a function of electrochemical oxidation time was explored as presented in Fig. 4. It can be seen that the length of $Cu(OH)_2$ nanoneedles gradually grew from around 1.8 μm at 2 min to about 5 μm at 6 min (Fig. 5a). In addition, the quantity of $Cu(OH)_2$ nanoneedles on the surface of copper mesh was evidently improved within 6 min, in agreement with the increasing atomic number ratio of O to Cu from 0.59:1 to 1.94:1 (Fig. 4a3, b3, c3). This phenomenon could be explained by the Faraday's first law of electrolysis (Eq. (8)).

$$m = k\mathrm{It} \tag{8}$$

where m is the mass of deposition at the anode, I and t are corresponding to the current and time [19].

The resultant smaller pore size of CM is supposed to be more favorable for the entrapment of oily liquids. As expected, the WCA reduced from about 42.3° to 0° and the underwater OCA toward kerosene was improved from 155.6° to appropriate 164.9° with extending anodization time from 2 to 6 min (Fig. 5b). Consequently, using the CM anodized for 6 min highest separation efficiency (99.5–99.8%) was obtained for mixture of water and various oils (gasoline, kerosene, diesel, hexane, bean oil and DCM) (Fig. 5c).

It is noteworthy that if the electrochemical oxidation time extended to 8 min, the nanoneedles no longer grew in length but the CM surface became much denser with more nanoneedles formed (Fig. 4d1, d2). Although with plenty of superhydrophilic —OH groups (Fig. 4d3), the porosity for capturing water to repel oily liquids tends to reduce, resulting in no further enhancement in the underwater superoleophobicity and oil/water separation efficiency (Fig. 5b, c).

3.3.2. Influence of current density

Moderate current density is essential to control the nucleation and growth processes of $Cu(OH)_2$ aiming for desired crystallinity and microstructure. It can be clearly observed that the pore size of CM gradually decreased with increasing current density (Fig. 6). This should be due to the various growth dimension, number density and nanostructures of $Cu(OH)_2$ nanoneedles. The nanoneedles obtained at a current density of 2 mA/cm^2 were sparse and short (~1 μm), with a lowest atomic ratio of O to Cu (1.27:1) (Fig. 6b3). Comparatively, the longest nanoneedles (~5 μm) were realized at 4 mA/cm^2 and the CM surface was almost completely covered by the nanoneedles. Whereas, as current density was as high as 6 mA/cm^2, the $Cu(OH)_2$ nanoneedles became thicker and shorter (~4 μm) (Fig. 5d). Some nanoneedles were inclined to aggregate to form bud-like bundles, causing the uneven morphology and lower coverage of coated CM surface. In conclusion, the best superhydrophilicity and underwater superoleophobicity for oil/water separation was achieved at 4 mA/cm^2 after 6 min oxidation (Fig. 5e, f).

It should be stated that various metal oxide or hydroxides have been previously created on metal substrates for oil/water

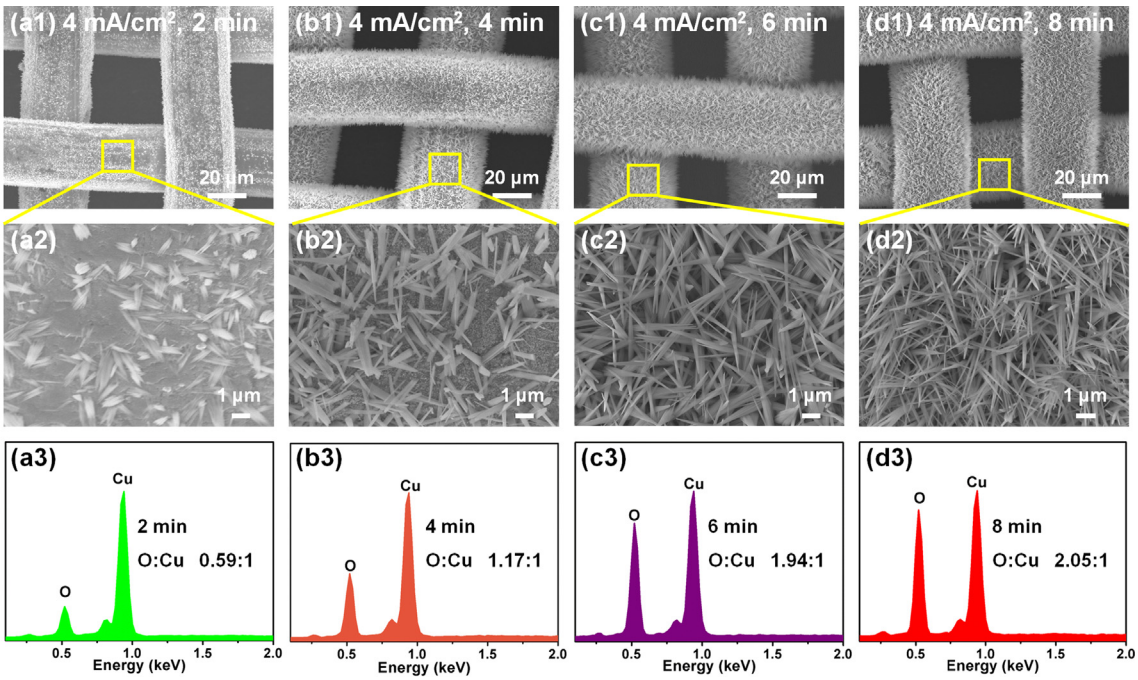

Fig. 4. Different magnification SEM images and EDS spectra of $Cu(OH)_2$/CM after anodic oxidation for (a1, a2, a3) 2 min, (b1, b2, b3) 4 min, (c1, c2, c3) 6 min and (d1, d2, d3) 8 min at 4 mA/cm^2.

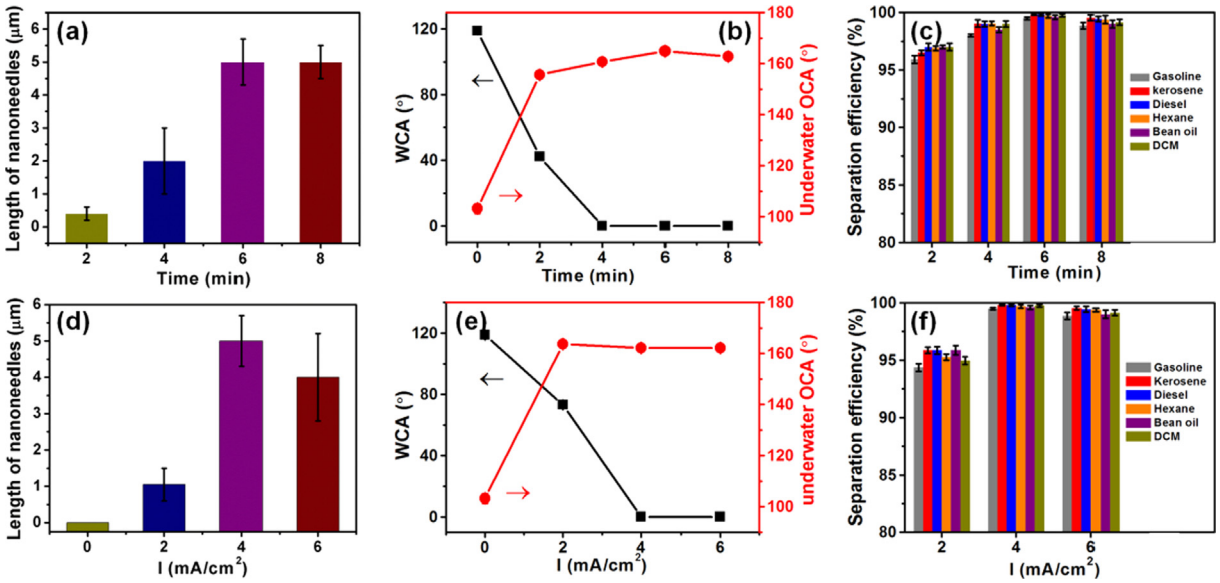

Fig. 5. Statistical curve of $Cu(OH)_2$ nanoneedles length as a function of (a) electrochemical reaction time and (d) current density. Influences of (b, c) reaction time and (e, f) current density on the wettability behaviors and oil/water separation efficiency of $Cu(OH)_2$/CM.

separation. For instance, Yuan et al. [48] fabricated nanostructured TiO_2/CuO dual coatings on CM by electrochemical anodization at 2 mA/cm^2 for 30 min and afterwards layer-by-layer self-assembly deposition to render superhydrophilic and underwater superoleophobic surface. Gao et al. [9] prepared microstructured TiO_2-based mesh through hydrothermal approach at 160 °C for 2 h combined with modification by octadecyl phosphonic acid. Comparatively, the strategy in this work has unique advantages of time-saving and easy-operation, which promise great potential in large-scale application.

3.4. Oil/water separation performance

The oil/water separation was automatically performed using the customized continuous running unit (Fig. 7a). Water could rapidly permeate through the pre-wetted mesh merely under gravity, while the oil was repelled by the superoleophobic mesh and thus effectively blocked above the mesh, achieving almost complete separation of water/kerosene mixture (~99.8%). Noticeably, the used mesh would become clean again once it is immersed in water, suggesting its low adhesion to the oil droplet. Extremely

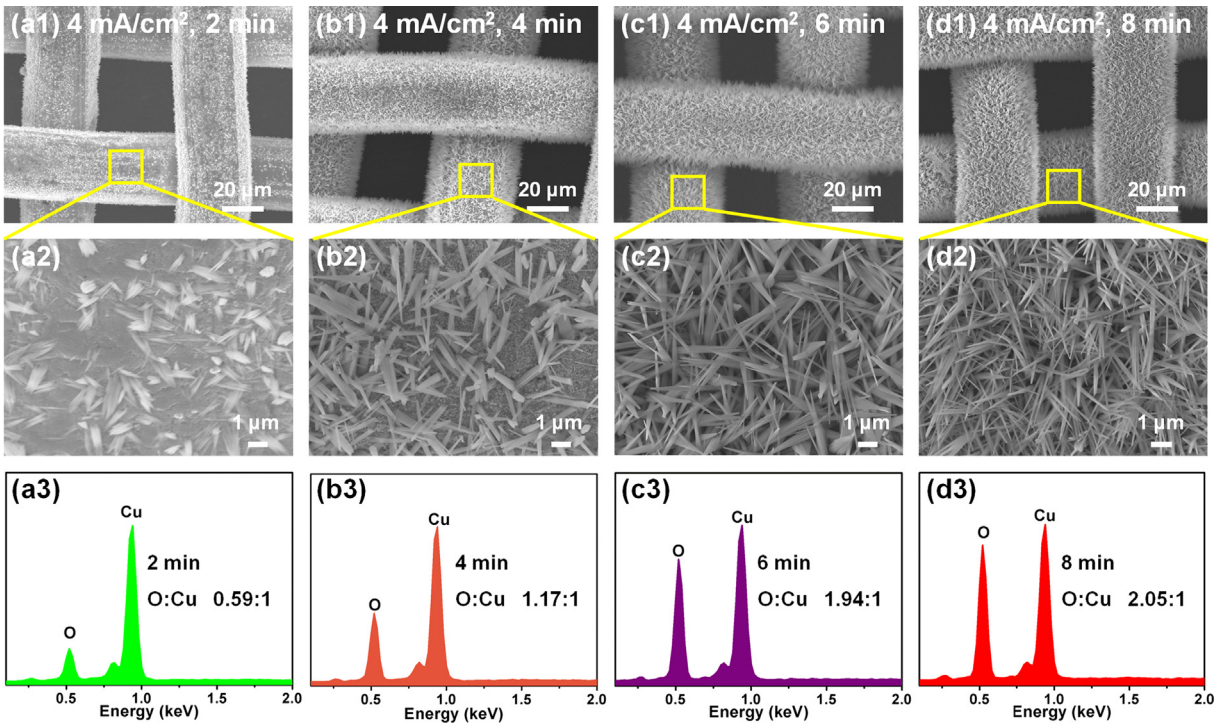

Fig. 6. Different magnification SEM images and EDS spectra of $Cu(OH)_2$/CM after anodic oxidation for 6 min at (a1, a2, a3) 0 mA/cm^2, (b1, b2, b3) 2 mA/cm^2, (c1, c2, c3) 4 mA/cm^2 and (d1, d2, d3) 6 mA/cm^2.

high separation efficiencies of greater than 99.5% were also obtained for mixtures of water and other oils (gasoline, diesel, hexane, bean oil and DCM), suggesting the wide range applications of the designed $Cu(OH)_2$/CM. To the best of knowledge, the $Cu(OH)_2$/CM in this study possesses superior oil/water separation performance compared with the recently reported separation membranes as listed in Table 1, such as MnO_2 nanocrystal (96%) [47], supramolecular hydrogel network (98.7%) [29] and SiO_2 nanoparticles (99%) [13] coated stainless steel meshes.

The oil/water separation process proceeds with the coalescence of oil droplets and come-up of the larger oil droplets. Based on the similarity-intermiscibility theory, it is more difficult for the oil droplets with lower surface tension to break the water films on the mesh surface, which may be responsible for the large underwater OCA and high separation efficiency as seen in Fig. S4a and b. In addition, the variation of the oil/water separation performance is also likely related to the density and viscosity of oils, which could affect the rising velocity of oil droplets according to the Stokes' Law [49]. As presented in Fig. S4c and e, the underwater OCA is apparently negative correlated with the density and viscosity of oils. The light oil droplets with low viscosity are expected to enhance the separation ability (Fig. S4d and f) [50].

To better understand the separation ability of the as-prepared $Cu(OH)_2$/CM, another key parameter oil intrusion pressure (P) is evaluated. By measuring the maximum height (h_{max}) of oil liquid that the coated mesh can withstand, the intrusion pressure value can be attained according to the following equation [13]:

$$P = \rho g h_{max} \quad (9)$$

where ρ and g are the oil density and gravitational acceleration, respectively.

As shown in Fig. 7b, the maximum bearable height of diesel can arrive at 30 cm, and the corresponding intrusion pressure is calculated to be about 2.34 kPa, higher than that of MnO_2 (2.10 kPa) [47] and SiO_2 (1.38 kPa) [13] nanoparticles coated stainless steel meshes. Moreover, the intrusion pressures of other oils (gasoline, kerosene, hexane, bean oil and DCM) are assessed to be above 1.30 kPa (Fig. 7c), revealing good stability of the coated mesh for practical oil/water separation.

In addition, the dynamic hydrophilicity of the coated mesh was examined by water permeating flux (F) measurements under a fixed column of water based on Eq. (10) [7,43]:

$$F = V/St \quad (10)$$

where V (L) is the volume of water permeating through the as-prepared mesh, here we fixed V to 0.2 L, S (m^2) is the effective surface area of the mesh on which the water flows, and t (s) is the required time for the permeation of 0.2 L water.

The water flux of $Cu(OH)_2$/CM could achieve as high as 191 160 L·m^{-2}h^{-1}, which is the highest value in comparison with the reported data (Table 2), for instance, SiO_2 nanoparticles (26 280 L·m^{-2}h^{-1}) [13] and diatomite (27 000 L·m^{-2}h^{-1}) [53] coated stainless steel meshes as well as TiO_2/CuO (80 000 L·m^{-2}h^{-1}) [48] and $Cu(OH)_2$ nanowires (158 000 L·m^{-2}h^{-1}) [25] coated copper meshes. It is noteworthy that the pristine CM exhibits a lower permeating flux (40 250 L·m^{-2}h^{-1}). According to the theory of Hagen-Poiseuille, the exceptional ultrahigh flux of the coated mesh can be reasonably attributed to the ultrathin monolayer of copper wires as well as substantial enhancement of the hydrophilicity without significantly sacrificing the effective average pore size [6,55]. Thereby, the as-prepared $Cu(OH)_2$/CM in this work would possess prominent advantage on the rapid separation of large amounts of oil/water mixtures.

3.5. Chemical resistance and stability

3.5.1. Chemical durability

Chemical resistance of the separation mesh is a key parameter for application in harsh environments and is thus evaluated by immersion in solutions with different pH (pH = 1–14) for 24 h. As

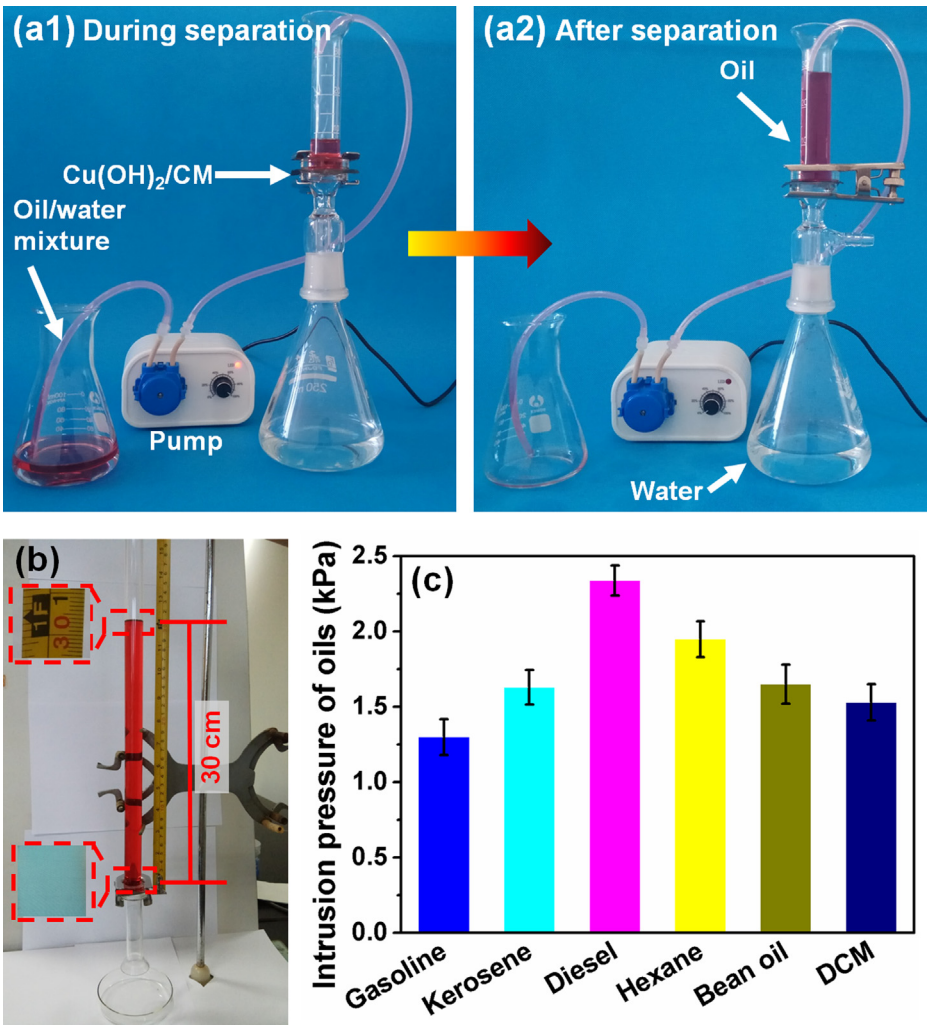

Fig. 7. (a1, a2) Separation process of oil/water mixture using $Cu(OH)_2$/CM. (b) Maximum height of oil column taking diesel as an example and (c) the intrusion pressure of $Cu(OH)_2$/CM for various oils.

Table 1
Comparison of the separation efficiency of $Cu(OH)_2$/CM in this work and other reported separation membranes.

No.	Separation membrane	Preparation method	Separation efficiency	Reference
1	Titania nanowires coated Ti mesh	Hydrothermal method	>96%	[7]
2	MnO_2 nanocrystal coated stainless steel mesh	Hydrothermal method	>96.2%	[47]
3	Copper coated fabrics	Modified hydrazine-assisted reduction method	>98%	[51]
4	Supramolecular hydrogel network coated stainless steel mesh	*In situ* radical polymerization	>98.7%	[29]
5	Zn-ZnO electrodeposited copper mesh	Electrodeposition	>99%	[19]
6	SiO_2 nanoparticles coated stainless steel mesh	Spraying method	>99%	[13]
7	TiO_2 nanoparticles coated stainless steel mesh	Spraying method	>99%	[52]
8	Diatomite coated stainless steel mesh	Spraying method	>99.2%	[53]
9	$Cu(OH)_2$ nanoneedles coated copper mesh	One-step anodic oxidation	>99.5%	This work

demonstrated in Fig. 8a, when the solution pH was below 2, the coated mesh lost its superhydrophilicity and the OCA reduced to 147°. As a consequence, the mesh could not effectively separate oil from water (Fig. 8b). It is found that under highly acidic conditions (pH = 1, 2) the long and densely arrayed nanoneedles completely disappeared due to acid-base neutralization reaction between $Cu(OH)_2$ and high amount of H^+ ions (Fig. 8c, d). However, at pH 3 the $Cu(OH)_2$ nanoneedles retained to a large extent although become shorter because of the corrosive effect of H^+ (Fig. 8e), which accounts for the high underwater superoleophobicity after immersion.

As the solution pH was changed from 4 to 14, the $Cu(OH)_2$/CM could maintain superhydrophilicity and underwater superoleophobicity (>160°) with small fluctuations, contributing to the almost unchanged separation efficiency. The well-preserved $Cu(OH)_2$ nanoneedles on CM surface can be clearly observed as the solution pH is 4 (Fig. 8f) or even up to 14 (inset of Fig. 8a), suggesting the extraordinary stability of the mesh within a broad pH range.

Then the separation efficiency of $Cu(OH)_2$/CM at extremely high salt concentrations was investigated as the anti-corrosive ability is of great importance for practical complicated environment [6,19].

Table 2
Comparison of the water permeating flux of $Cu(OH)_2$/CM in this work and other reported separation membranes.

No.	Separation membrane	Preparation method	Flux ($L·m^{-2}h^{-1}$)	Reference
1	Ti foam coated by fluorinated hierarchical flower-like TiO_2 nanostructures	One-step hydrothermal method	2 174	[54]
2	MoS_2-coated fabric	Impregnation method	6 120	[30]
3	P(AM-*co*-AA)/CS/MPS-SiO_2 nanocomposite hydrogel	Free-radical polymerization method	8 600	[31]
4	TiO_2 nanowires coated stainless steel	Dip-coating method	11 000	[23]
5	Cellulose hydrogel coated wire mesh	*In situ* radical polymerization	12 885	[6]
6	Catechol deposited PVDF membrane	Immersion method	21 000	[55]
7	SiO_2 nanoparticles coated stainless steel mesh	Spraying method	26 280	[13]
8	Diatomite coated stainless steel mesh	Spraying method	27 000	[19]
9	Nanostructured TiO_2/CuO Dual-coated copper mesh	Electrochemical anodization and layer-by-layer self-assembly deposition	100 000	[48]
10	$Cu(OH)_2$ coated copper mesh	Solution immersion method	120 000	[22]
11	$Cu(OH)_2$ nanowire-haired copper mesh	Solution immersion method	158 000	[25]
12	$Cu(OH)_2$ nanoneedles coated copper mesh	One-step anodic oxidation	191 160	This work

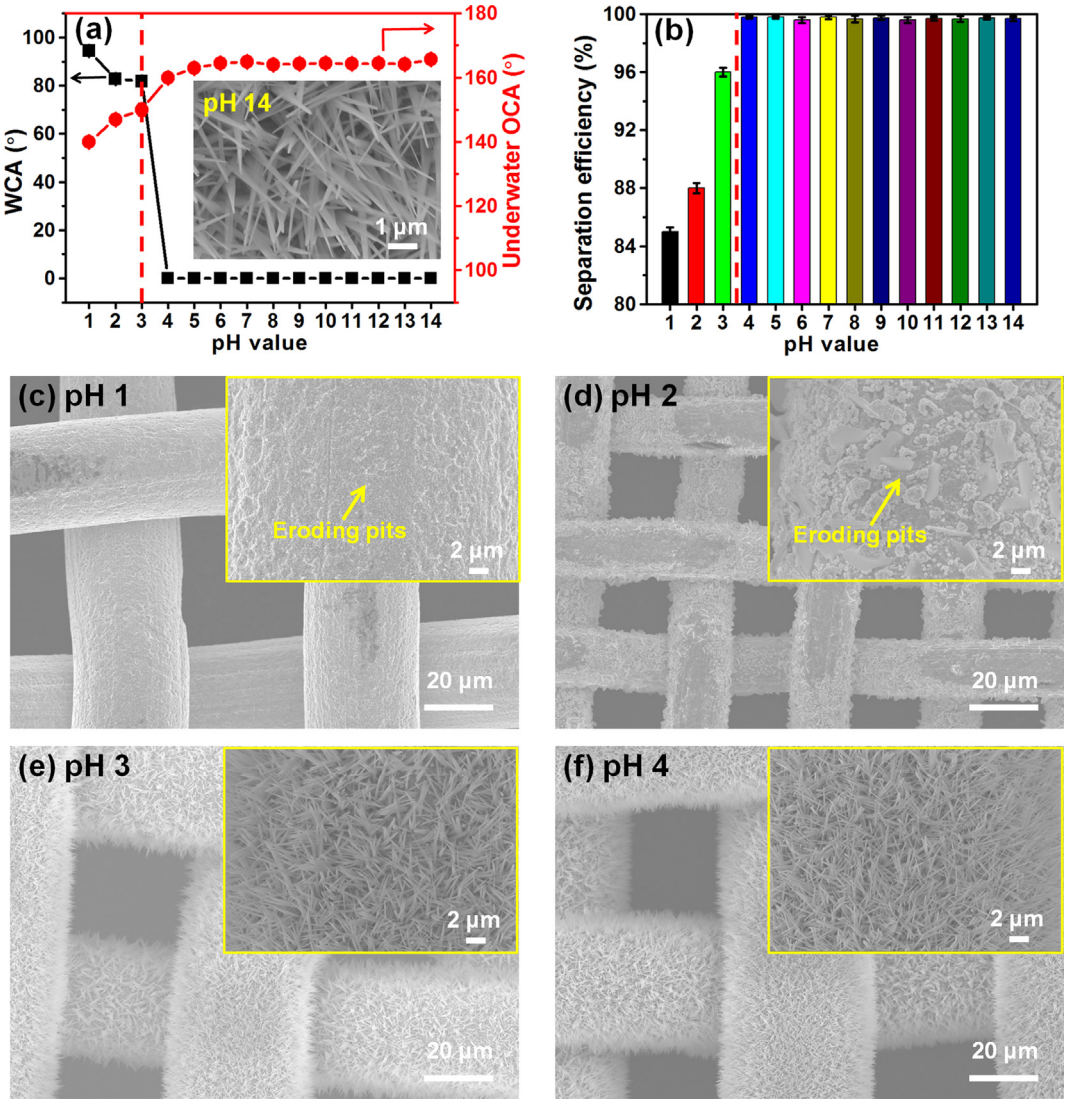

Fig. 8. (a) Variation of WCA and underwater OCA and (b) oil/water separation efficiency of $Cu(OH)_2$/CM after immersing in solution with different pH values (kerosene as oil model). The SEM images of the $Cu(OH)_2$/CM after immersing in solution with different pH values for 24 h: Inset of (a) pH = 14, (c) pH = 1, (d) pH = 2, (e) pH = 3, (f) pH = 4.

As shown in Fig. 9a, the saturated NaCl solution could rapidly penetrate through the mesh, while the oil (kerosene) was repelled beyond the mesh surface, demonstrating high separation efficiency of over 99.5%. No visible colored oil was observed in the water after separation. The superhydrophilicity and underwater superoleophobicity of the separation mesh can be even kept after immersion in saturated NaCl solution for 24 h, and efficient separation efficiency of approximately 99.3% was reached for kerosene/water

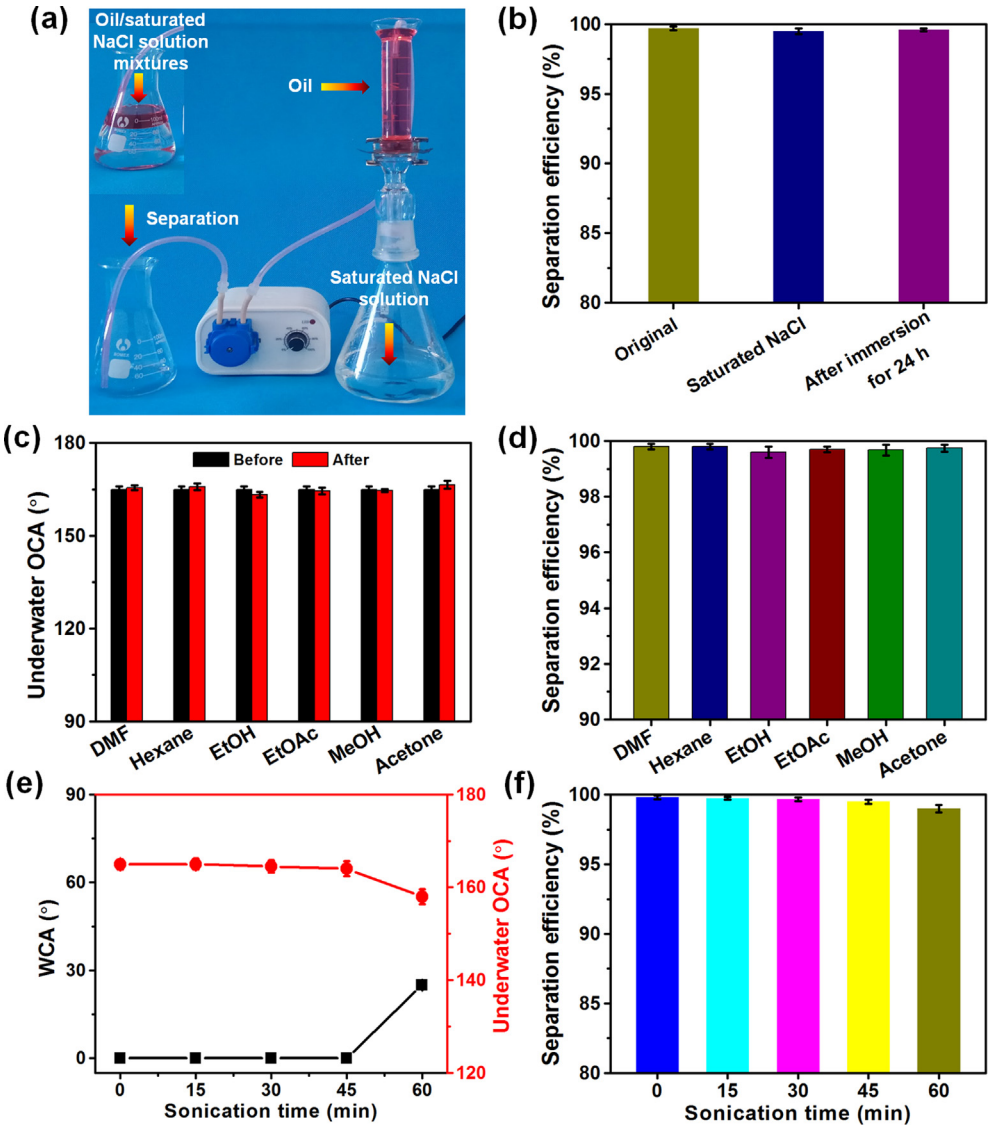

Fig. 9. (a) Separation process and (b) separation efficiency of $Cu(OH)_2$/CM in saturated NaCl solution environment. (c) The underwater OCA and (d) oil/water separation efficiency of $Cu(OH)_2$/CM after immersing in various organic solvents for 24 h. (e) The wettability behaviors and (f) oil/water separation efficiency of $Cu(OH)_2$/CM after sonication for different time (kerosene as oil model).

mixture (Fig. 9b). This promises $Cu(OH)_2$/CM particular potential application in remediation of high salinity oily wastewater or marine oil leakage.

The solvent resistance of $Cu(OH)_2$/CM was tested by submerging the mesh in six common organic solvents for 24 h, including DMF, EtOH, EtOAc, MeOH, hexane and acetone. As presented in Fig. 9c and d, The $Cu(OH)_2$/CM still retained underwater superoleophobicity with OCA of above 163.3° and separation efficiency of greater than 99.6% for kerosene/water mixture. Such remarkable anti-fouling ability of the $Cu(OH)_2$/CM is superior to polymer-dominated membranes [6,55].

3.5.2. Wear resistance

The cohesional strength of $Cu(OH)_2$ nanoneedles on CM surface is critical for long-term usage and is thus estimated under external force [56,57]. After 45 min of vigorous sonication treatment at 480 W, very few of $Cu(OH)_2$ nanoneedles were fallen from the CM substrate (Fig. S5a). The underwater OCA (kerosene as oil model) remained above 158° with small fluctuations (Fig. 9e), and the separation efficiency of more than 99% could also be achieved (Fig. 9f). After 60 min treatment, only a small number of nanoneedles were lost (Fig. S5b), leading to the reserved high underwater OCA of above 158° and separation efficiency of more than 99%. Such great cohesional strength should be related to the chemical attachment of $Cu(OH)_2$ nanoneedles to the mesh surface via in situ growth process [6].

Actual oily wastewaters, such as oil-field effluents and oil spill sewage, usually contain solid particles (i.e. sand), which may damage the surface topography of the mesh [58]. Thus, mechanical durability is regarded as crucial aspect for stable oil/water separation and thus estimated by sand abrasion test as presented in Fig. 10a. The sand grains with diameter of 180–250 μm were fallen from a height of 20 cm to impact the mesh with tilt angle of 45°. The surface topography of $Cu(OH)_2$/CM after being subject to 800 g sand abrasion test is shown in Fig. S6. It can be seen that although some areas of the mesh were polluted by the falling sand, most of the $Cu(OH)_2$ nanoneedles were well retained with slight damage. The robust microstructure of the mesh may be responsible for the preserved superhydrophilicity and underwater superoleophobicity as well as high separation efficiency of 98.5% for

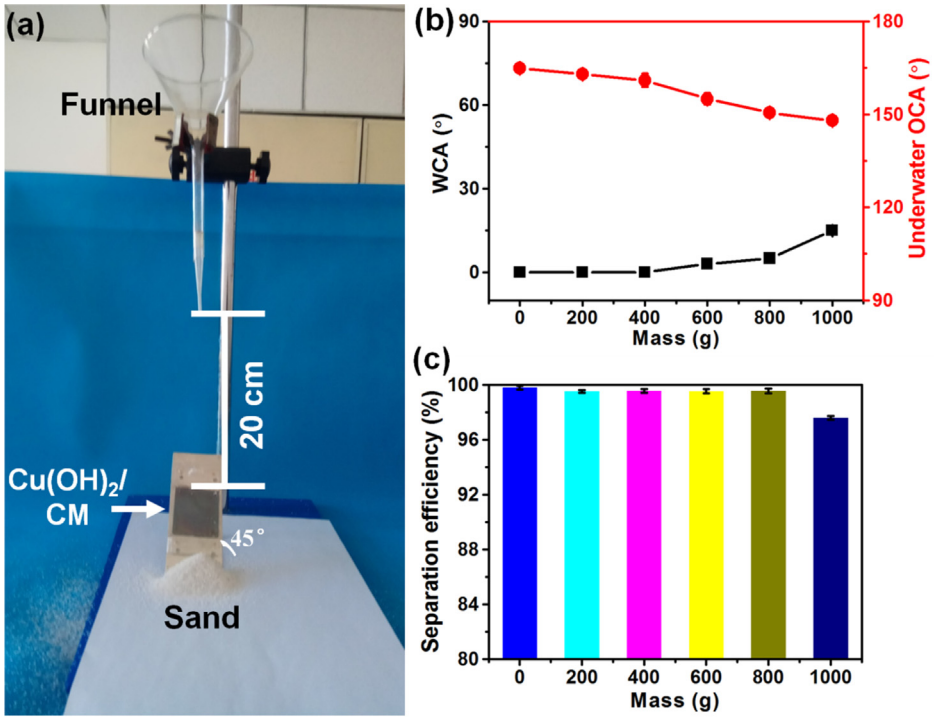

Fig. 10. (a) Photograph of sand abrasion test. (b) Wettability behaviors and (c) oil/water separation efficiency of $Cu(OH)_2$/CM after sand abrasion (kerosene as oil model).

kerosene/water mixture after abrasion test (Fig. 10b, c). The WCA of the coated mesh increased to about 15° after being subject to 1000 g sand, while the underwater OCA was higher than 148° and the separation efficiency was still above 97.6%. The aforementioned results reveal that the $Cu(OH)_2$/CM possesses prominent mechanical robustness to withstand mechanical challenges.

3.5.3. Heat stability

The thermogravimetric analysis (inset of Fig. 11a) reveals that the coated mesh demonstrates excellent thermal stability below 400 °C, with weight loss of less than 0.6%. The collapse of nanoneedles structure occurred at 150 °C arising from the conversion from blue $Cu(OH)_2$ to dark CuO as seen in Fig. S7 [25]. In the XRD pattern

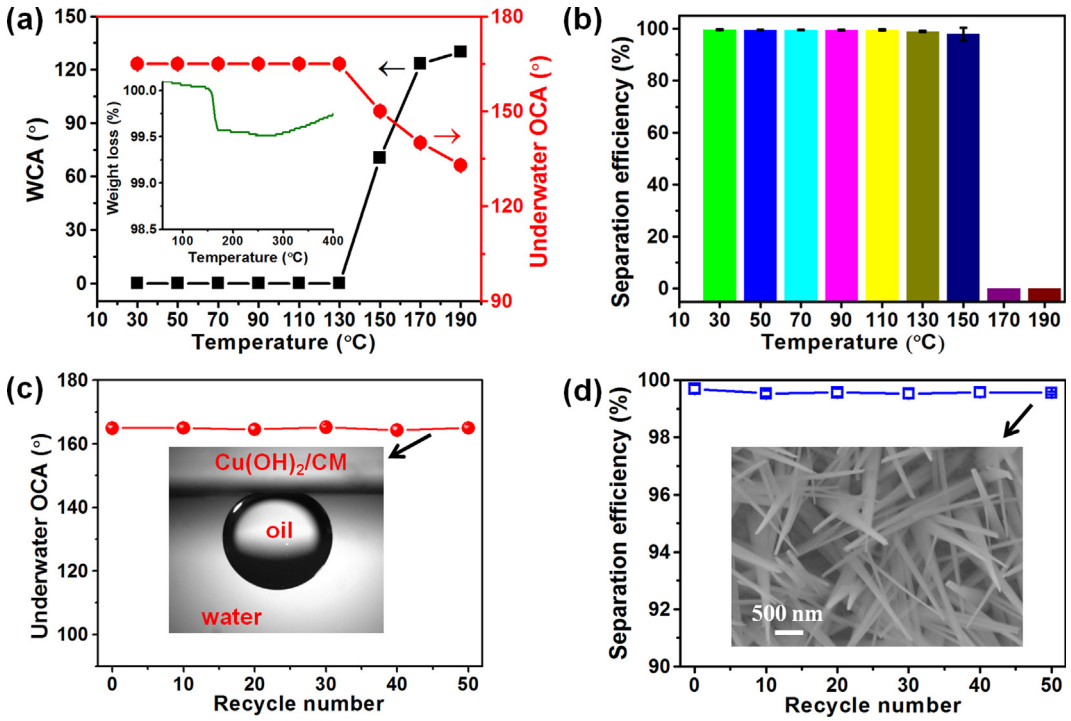

Fig. 11. (a) The variation of WCA and underwater OCA as a function of heating temperature. (b) The separation efficiency of $Cu(OH)_2$/CM for water/kerosene mixture after treated under different temperature. (c) The wettability behaviors and (d) oil/water separation efficiency of $Cu(OH)_2$/CM versus the recycle numbers. Inset of (a) is the TG curve of the $Cu(OH)_2$/CM. Inset of (c) is the kerosene droplet below the mesh surface in water. Inset of (d) is the SEM image of $Cu(OH)_2$/CM after 50 runs.

of the mesh after treated at 150 °C (Fig. S8), the characteristic peaks of $Cu(OH)_2$ at 21.6° (0 2 0) and 23.74°(0 2 1) completely disappeared, while the weak diffraction peaks at 35.52° (0 0 2) and 38.71° (1 1 1) can be ascribed to the monoclinic phase of CuO (JCPDS Card no. 05-0661). From the EDS spectra (Fig. S9) the atomic number ratio of O to Cu decreased from 1.94:1 to 1.10:1, which is close to the theoretical value of CuO. The WCA and underwater OCA of the coated mesh were also measured after heating at certain temperature for 1 h. It is found that the coated mesh could maintain the superhydrophilicity and underwater superoleophobicity below 150 °C (Fig. 11a). The residual high separation efficiency of above 98% (Fig. 11b) and the well-preserved nanoneedles-like morphology (Fig. S7) indicates the good stability of the mesh.

3.5.4. Recycling ability

The reusability of the $Cu(OH)_2$/CM was examined using kerosene as the oil model in the present study. As shown in Fig. 11c and d, underwater superoleophobic property (OCA > 163°) and high separation efficiency of above 99.5% was still achieved even after 50 cycles with no observable oil in the collected water, demonstrating outstanding recyclability of the as-prepared copper mesh. In addition, extremely high flux of the mesh could be well maintained after 50 cycles (~191 050 $L{\cdot}m^{-2}h^{-1}$) (Fig. S10), suggesting the potential operation stability for long time usage. As displayed in the inset SEM image of Fig. 11d, the microstructure morphology of the used mesh after 50 runs remained almost unchanged, which implies the durability of the designed $Cu(OH)_2$ nanoneedles. Moreover, the long-term anti-oil property of the $Cu(OH)_2$/CM surface was examined as seen in Fig. S11. The oil droplet (kerosene) retained approximate spherical shape without any spreading for a long time (24 h). This further implies the stable anti-oil ability of the mesh, which may contribute to the high stability in multiple usages.

3.6. Separation mechanism

The micropores in $Cu(OH)_2$/CM with size of about 20 μm, which are according with capillary mechanics, could act as the abundant capillary tubes during oil/water separation process [59]. The Jurin height of the mesh was calculated to be around 1.3 m based on the Jurin's formula (Eq. (11)) [60].

$$h_{max} = \frac{2\gamma\cos\theta}{R\rho g} \tag{11}$$

where γ is the surface tension of liquid, R is the radius of capillary, θ is the intrinsic contact angle of liquid on the surface, ρ is the density of liquid, g is the acceleration of gravity.

The Jurin height is far greater than the thickness of the superhydrophilic mesh (<100 μm). Thus, the water is prone to penetrate through the mesh micropores while the oil molecules easily rise up because of upward pressure induced by capillary. This would finally favor the continuous separation of oil and water [59].

To in-deep understand the oil/water separation mechanism, the wetting process of water and oil on the $Cu(OH)_2$ nanoneedles coated copper mesh is modeled based on the concept of intrusion pressure as illustrated in Fig. 12. The theoretical intrusion pressure (ΔP) can be calculated using Eq. (12), which has been widely applied to investigate the oil/water separation mechanisms of membranes [38,58,61,62].

$$\Delta P = \frac{2\gamma}{R} = -\frac{C\gamma\cos\theta}{A} \tag{12}$$

where γ is the surface tension, R is the radius of the meniscus, C is the circumference of the mesh pore, θ is the water or oil contact angle on the coated mesh, and A is the cross-sectional area of the pore.

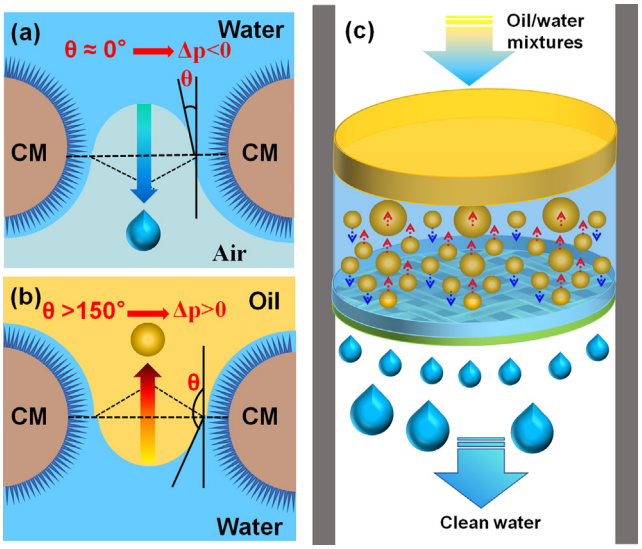

Fig. 12. Schematic illustration of oil/water separation: (a) superhydrophilicity in air and (b) underwater superoleophobicity of $Cu(OH)_2$/CM; (c) separation process of water/oil mixture.

As displayed in Fig. 12a, the ΔP should be less than zero as the water contact angle of the coated mesh is nearly 0°. Thus the water can easily enter the interspaces of the mesh wires and spontaneously permeate through the micropores of the mesh under the driven of gravity and capillary force (Δp < 0) [21]. Due to the preferential affinity of water with the membrane, a stable water/solid composite interface would be formed. The pre-wetted $Cu(OH)_2$/CM exhibits superoleophobicity in water (θ>150°), implying that the ΔP is higher than zero with negative capillary effect (Fig. 12b). Consequently, the micro-sized oil droplets can be well hold by the hierarchical structured mesh under the action of intrusion pressure [63].

As presented in Fig. 12c, the dispersible oil droplets in the fluid would first move downwards with the water. Upon touching the superhydrophilic surface of the mesh, they can be blocked and then move in the opposite direction under the intrusion pressure and action of buoyancy. On the way up, the size of the oil droplets would gradually increase through the coalescence effect. Based on the Stokes' law, the rising velocity of oil droplet is positively related to its radius. Consequently, the oil droplets with larger radius are prone to float up to form oil layer, which can be collected and recycled after complete separation.

4. Conclusions

In summary, the $Cu(OH)_2$ nanoneedles coated copper mesh with inverse wettability was successfully constructed via facile anodic oxidation approach. High separation efficiency of above 99.5% was achieved for various oils/water mixtures with a ultrahigh water flux of 191 160 $L{\cdot}m^{-2}h^{-1}$ and intrusion pressure of over 1.30 kPa. The slight variation in separation efficiency without apparent change in microstructure after 50 cycles could afford the possibility of $Cu(OH)_2$/CM for excellent reusability.

In addition, the coated mesh exhibited extraordinary chemical resistance towards strongly base, saturated NaCl solution and common organic solvents, which would meet the requirements for oil/water separation under practical harsh environments. Moreover, the separation mesh could withstand mechanical challenges due to great cohesional strength of $Cu(OH)_2$ nanoneedles.

The as-prepared $Cu(OH)_2$/CM also possessed prominent advantages of high temperature durability in contrast to organic polymer based membranes. Thus, the separation mesh in this work has great potential for scalable applications in efficiently separating oils from most industrial fields or retrieving oil leakages in the ocean.

Acknowledgements

The research is financially supported by Funds for Postdoctoral Research Program of Heilongjiang Province (LBH-Z18043), Postgraduate Innovative Research Project from Northeast Petroleum University of China (JYCX_CX03_2018), Foundation of Guangzhou Key Laboratory of Environmental Catalysis and Pollution Control (GKLECPC-10), Cultivating Fund of National Science Foundation (2018GPQZ-06) and Outstanding Scientific Research Talents (SJQHB201902) from Northeast Petroleum University of China.

Appendix A. Supplementary material

Supplementary data to this article can be found online at https://doi.org/10.1016/j.jcis.2019.08.011.

References

[1] J. Ge, Q. Jin, D. Zong, J. Yu, B. Ding, Biomimetic multilayer nanofibrous membranes with elaborated superwettability for effective purification of emulsified oily wastewater, ACS Appl. Mater. Interf. 10 (2018) 16183–16192.
[2] Q. Ma, H. Cheng, Y. Yu, Y. Huang, Q. Lu, S. Han, J. Chen, R. Wang, A.G. Fane, H. Zhang, Preparation of superhydrophilic and underwater superoleophobic nanofiber-based meshes from waste glass for multifunctional oil/water separation, Small 13 (2017) 1700391.
[3] Y. Deng, G. Zhang, R. Bai, S. Shen, X. Zhou, I. Wyman, Fabrication of superhydrophilic and underwater superoleophobic membranes via an in situ crosslinking blend strategy for highly efficient oil/water emulsion separation, J. Membr. Sci. 569 (2019) 60–70.
[4] J. Ge, H.Y. Zhao, H.W. Zhu, J. Huang, L.A. Shi, S.H. Yu, Advanced sorbents for oil-spill cleanup: recent advances and future perspectives, Adv. Mater. 28 (2016) 10459–10490.
[5] Z. Yu, F.Y. Fei, Z. Gong, Q. Yao, S.X. Dou, K. Liu, L. Jiang, X. Wang, A novel reusable superhydrophilic NiO/Ni mesh produced by a facile fabrication method for superior oil/water separation, J. Mater. Chem. A 5 (2017) 10821–10826.
[6] C. Ao, R. Hu, J. Zhao, X. Zhang, Q. Li, T. Xia, W. Zhang, C. Lu, Reusable, salt-tolerant and superhydrophilic cellulose hydrogel-coated mesh for efficient gravity-driven oil/water separation, Chem. Eng. J. 338 (2018) 271–277.
[7] L. Zhang, Y. Zhong, D. Cha, P. Wang, A self-cleaning underwater superoleophobic mesh for oil-water separation, Sci. Rep. 3 (2013) 2326.
[8] W. Zhang, Y. Zhu, X. Liu, D. Wang, J. Li, L. Jiang, J. Jin, Salt-induced fabrication of superhydrophilic and underwater superoleophobic PAA-g-PVDF membranes for effective separation of oil-in-water emulsions, Angew. Chem. Int. Edit. 53 (2014) 856–860.
[9] C. Gao, Z. Sun, K. Li, Y. Chen, Y. Cao, S. Zhang, L. Feng, Integrated oil separation and water purification by a double-layer TiO_2-based mesh, Energ. Environ. Sci. 6 (2013) 1147–1151.
[10] Q. Ma, H. Cheng, A.G. Fane, R. Wang, H. Zhang, Recent development of advanced materials with special wettability for selective oil/water separation, Small 12 (2016) 2186–2202.
[11] B. Su, T. Ye, J. Lei, Bioinspired interfaces with superwettability: from materials to chemistry, J. Am. Chem. Soc. 138 (2016) 1727–1748.
[12] S. Zhang, G. Jiang, S. Gao, H. Jin, Y. Zhu, F. Zhang, J. Jin, Cupric phosphate nanosheets-wrapped Inorganic membranes with superhydrophilic and outstanding anticrude oil-fouling property for oil/water separation, ACS Nano 12 (2018) 795–803.
[13] J. Li, D. Li, W. Li, H. Li, H. She, F. Zha, Facile fabrication of underwater superoleophobic SiO_2 coated meshes for separation of polluted oils from corrosive and hot water, Sep. Purif. Technol. 168 (2016) 209–214.
[14] J. Wang, H. Wang, Integrated device based on cauliflower-like nickel hydroxide particles-coated fabrics with inverse wettability for highly efficient oil/hot alkaline water separation, J. Coll. Interf. Sci. 534 (2019) 228–238.
[15] M. Liu, S. Wang, Z. Wei, Y. Song, L. Jiang, Bioinspired design of a superoleophobic and low adhesive water/solid interface, Adv. Mater. 21 (2009) 665–669.
[16] Q. Wen, J. Di, L. Jiang, J. Yu, Xu Ruren, Zeolite-coated mesh film for efficient oil-water separation, Chem. Sci. 4 (2013) 591–595.
[17] C. Zhou, J. Cheng, K. Hou, A. Zhao, P. Pi, X. Wen, S. Xu, Superhydrophilic and underwater superoleophobic titania nanowires surface for oil repellency and oil/water separation, Chem. Eng. J. 301 (2016) 249–256.
[18] Z. Xue, S. Wang, L. Lin, L. Chen, M. Liu, L. Feng, L. Jiang, A novel superhydrophilic and underwater superoleophobic hydrogel-coated mesh for oil/water separation, Adv. Mater. 23 (2011) 4270–4273.
[19] Q. You, G. Ran, C. Wang, Y. Zhao, Q. Song, A novel superhydrophilic–underwater superoleophobic Zn-ZnO electrodeposited copper mesh for efficient oil/water separation, Sep. Purif. Technol. 193 (2018) 21–28.
[20] H. Ahn, H. Lee, S. Lee, Y. Lee, Dehydration of TFEA/water mixture through hydrophilic zeolite membrane by pervaporation, J. Membr. Sci. 291 (2007) 46–52.
[21] J. Ge, J. Zhang, F. Wang, Z. Li, J. Yu, B. Ding, Superhydrophilic and underwater superoleophobic nanofibrous membrane with hierarchical structured skin for effective oil-in-water emulsion separation, J. Mater. Chem. A 5 (2017) 497–502.
[22] H. Lai, X. Yu, M. Liu, Z. Cheng, One-step solution immersion process for the fabrication of low adhesive underwater superoleophobic copper mesh film toward high-flux oil/water separation, Appl. Surf. Sci. 448 (2018) 241–247.
[23] Z. Pan, S. Cao, J. Li, Z. Du, F. Cheng, Anti-fouling TiO_2 nanowires membrane for oil/water separation: synergetic effects of wettability and pore size, J. Membr. Sci. 572 (2019) 596–606.
[24] X. Du, X. Huang, X. Li, X. Meng, L. Yao, J. He, H. Huang, X. Zhang, Wettability behavior of special microscale ZnO nail-coated mesh films for oil–water separation, J. Coll. Interf. Sci. 458 (2015) 79–86.
[25] F. Zhang, W. Zhang, Z. Shi, D. Wang, J. Jin, L. Jiang, Nanowire-haired inorganic membranes with superhydrophilicity and underwater ultralow adhesive superoleophobicity for high-efficiency oil/water separation, Adv. Mater. 25 (2013) 4192–4198.
[26] Y. Liu, Y. Zhang, X. Fu, H. Sun, Bioinspired underwater superoleophobic membrane based on a graphene oxide coated wire mesh for efficient oil/water separation, ACS Appl. Mater. Interf. 7 (2015) 20930–20936.
[27] J. Zeng, Z. Guo, Superhydrophilic and underwater superoleophobic MFI zeolite-coated film for oil/water separation, Colloid Surface. A 444 (2014) 283–288.
[28] Q. Cheng, C. Guan, M. Wang, Y. Li, J.B. Zeng, Cellulose nanocrystal coated cotton fabric with superhydrophobicity for efficient oil/water separation, Carbohyd. Polym. 199 (2018) 390–396.
[29] Y. Liu, M. Su, Y. Fu, P. Zhao, M. Xia, Y. Zhang, B. He, P. He, Corrosive environments tolerant, ductile and self-healing hydrogel for highly efficient oil/water separation, Chem. Eng. J. 354 (2018) 1185–1196.
[30] Y. Dong, C. Huang, X. Yang, Underwater superoleophobic and underoil superhydrophobic surface made by liquid-exfoliated MoS_2 for on-demand oil-water separation, Chem. Eng. J. 361 (2019) 322–328.
[31] M. Su, Y. Liu, S. Li, Z. Fang, B. He, Y. Zhang, Y. Li, P. He, A rubber-like, underwater superoleophobic hydrogel for efficient oil/water separation, Chem. Eng. J. 361 (2019) 364–372.
[32] J. Ge, D. Zhong, Q. Jin, J. Yu, B. Ding, Biomimetic and superwettable nanofibrous skins for highly efficient separation of oil-in-water emulsions, Adv. Funct. Mater. 28 (2018) 1705051.
[33] M. Khosravi, S. Azizian, R. Boukherroub, Efficient oil/water separation by superhydrophobic Cu_xS coated on copper mesh, Sep. Purif. Technol. 215 (2019) 573–581.
[34] C.R. Crick, J.A. Gibbins, I.P. Parkin, Superhydrophobic polymer-coated copper-mesh; membranes for highly efficient oil–water separation, J. Mater. Chem. A. 1 (2013) 5943–5948.
[35] H. Zhu, P. Guo, Z. Shang, X. Yu, Y. Zhang, Fabrication of underwater superoleophobic metallic fiber felts for oil-water separation, Appl. Surf. Sci. 447 (2018) 72–77.
[36] M. Liu, J. Li, Z. Guo, Electrochemical route to prepare polyaniline-coated meshes with controllable pore size for switchable emulsion separation, Chem. Eng. J. 304 (2016) 115–120.
[37] J. Liu, L. Wang, N. Wang, F. Guo, L. Hou, Y. Chen, J. Liu, Y. Zhao, L. Jiang, A robust $Cu(OH)_2$ nanoneedles mesh with tunable wettability for nonaqueous multiphase liquid separation, Small 13 (2017) 1600499.
[38] W. Ma, M. Zhang, Z. Liu, C. Huang, G. Fu, Nature-inspired creation of a robust free-standing electrospun nanofibrous membrane for efficient oil–water separation, Environ. Sci-Nano. 5 (2018) 2909–2920.
[39] M. Zhang, W. Ma, S. Wu, G. Tang, J. Cui, Q. Zhang, F. Chen, R. Xiong, C. Huang, Electrospun frogspawn structured membrane for gravity-driven oil-water separation, J. Coll. Interf. Sci. 547 (2019) 136–144.
[40] Z. Chu, S. Seeger, Superamphiphobic surfaces, Chem. Soc. Rev. 43 (2014) 2784–2798.
[41] X. Wang, M. Li, Y. Shen, Y. Yang, H. Feng, J. Li, Facile preparation of loess-coated membranes for multifunctional surfactant-stabilized oil-in-water emulsion separation, Green. Chem. 21 (2019) 3190–3199.
[42] Y. Long, Y. Shen, H. Tian, Y. Yang, H. Feng, J. Li, Superwettable Coprinus comatus coated membranes used toward the controllable separation of emulsified oil/water mixtures, J. Membr. Sci. 565 (2018) 85–94.
[43] S.Y. Khew, C.F. Tan, H. Yan, S. Lin, E.S. Thian, R. Zhou, M. Hong, Nanosecond laser ablation for enhanced adhesion of CuO nanowires on copper substrate and its application for oil-water separation, Appl. Surf. Sci. 465 (2019) 995–1002.
[44] Y. Lu, S. Sathasivam, J. Song, C.R. Crick, C.J. Carmalt, I.P. Parkin, Robust self-cleaning surfaces that function when exposed to either air or oil, Science 347 (2015) 1132–1135.
[45] J. Li, C. Xu, C. Guo, H. Tian, F. Zha, L. Guo, Underoil superhydrophilic desert sand layer for efficient gravity-directed water-in-oil emulsions separation with high flux, J. Mater. Chem. A 6 (2018) 223–230.

[46] J. Wang, H. Wang, Easily enlarged and coating-free underwater superoleophobic fabric for oil/water and emulsion separation via a facile $NaClO_2$ treatment, Sep. Purif. Technol. 195 (2018) 358–366.
[47] J. Wang, F. Han, Y. Chen, H. Wang, A pair of MnO_2 nanocrystal coatings with inverse wettability on metal meshes for efficient oil/water separation, Sep. Purif. Technol. 209 (2019) 119–127.
[48] S. Yuan, C. Chen, A. Raza, R. Song, T.J. Zhang, S.O. Pehkonen, B. Liang, Nanostructured TiO_2/CuO dual-coated copper meshes with superhydrophilic, underwater superoleophobic and self-cleaning properties for highly efficient oil/water separation, Chem. Eng. J. 328 (2017) 497–510.
[49] S. Deng, R. Bai, J.P. Chen, Z. Jiang, G. Yu, F. Zhou, Z. Chen, Produced water from polymer flooding process in crude oil extraction: characterization and treatment by a novel crossflow oil-water separator, Sep. Purif. Technol. 29 (2002) 207–216.
[50] Z. Chu, Y. Feng, S. Seeger, Oil/Water Separation with selective superantiwetting/superwetting surface materials, Angew. Chem. Int. Ed. 53 (2014) 2–13.
[51] W. Yang, J. Li, P. Zhou, L. Zhu, H. Tang, Superhydrophobic copper coating: switchable wettability, on-demand oil-water separation, and antifouling, Chem. Eng. J. 327 (2017) 849–854.
[52] J. Li, L. Yan, W. Hu, D. Li, F. Zha, Z. Lei, Facile fabrication of underwater superoleophobic TiO_2 coated mesh for highly efficient oil/water separation, Colloid Surface. A 489 (2016) 441–446.
[53] J. Li, P. Guan, Y. Zhang, B. Xiang, X. Tang, H. She, A diatomite coated mesh with switchable wettability for on-demand oil/water separation and methylene blue adsorption, Sep. Purif. Technol. 174 (2017) 275–281.
[54] B. Jiang, Z. Chen, H. Dou, Y. Sun, H. Zhang, Z. Gong, L. Zhang, Superhydrophilic and underwater superoleophobic Ti foam with fluorinated hierarchical flower-like TiO_2 nanostructures for effective oil-in-water emulsion separation, Appl. Surf. Sci. 456 (2018) 114–123.
[55] Y. Chen, Q. Liu, Oxidant-induced plant phenol surface chemistry for multifunctional coatings: Mechanism and potential applications, J. Membr. Sci. 570 (2019) 176–183.
[56] L. Xu, D. Zhu, X. Lu, Q. Lu, Transparent, thermally and mechanically stable superhydrophobic coating prepared by an electrochemical template strategy, J. Mater. Chem. A 3 (2015) 3801–3807.
[57] H. Zhou, H. Wang, H. Niu, Y. Zhao, Z. Xu, T. Lin, A waterborne coating system for preparing robust, self-healing, superamphiphobic surfaces, Adv. Funct. Mater. 27 (2017) 1604261.
[58] J. Wang, H. Wang, One-step fabrication of coating-free mesh with underwater superoleophobicity for highly efficient oil/water separation, Surf. Coat. Tech. 340 (2018) 1–7.
[59] J. Cui, Z. Zhou, A. Xie, M. Meng, Y. Cui, S. Liu, J. Lu, S. Zhou, Y. Yan, H. Dong, Bio-inspired fabrication of superhydrophilic nanocomposite membrane based on surface modification of SiO_2 anchored by polydopamine towards effective oil-water emulsions separation, Sep. Purif. Technol. 209 (2019) 434–442.
[60] A. Xie, J. Cui, Y. Chen, J. Lang, C. Li, Y. Yan, J. Dai, Capillarity-driven both light and heavy oil/water separation via combined system of opposite superwetting meshes, Sep. Purif. Technol. 215 (2019) 1–9.
[61] W. Ma, M. Zhang, Z. Liu, M. Kang, C. Huang, G. Fu, Fabrication of highly durable and robust superhydrophobic-superoleophilic nanofibrous membranes based on a fluorine-free system for efficient oil/water separation, J. Membr. Sci. 570 (2019) 303–313.
[62] W. Ma, J. Zhao, O. Oderinde, J. Han, Z. Liu, B. Cao, R. Xiong, Q. Zhang, S. Jiang, C. Huang, Durable superhydrophobic and superoleophilic electrospun nanofibrous membrane for oil-water emulsion separation, J. Coll. Interf. Sci. 532 (2018) 12–23.
[63] W. Ma, S.K. Samal, Z. Liu, R. Xiong, S.C. De Smedt, B. Bhushan, Q. Zhang, C. Huang, Dual pH-and ammonia-vapor-responsive electrospun nanofibrous membranes for oil-water separations, J. Membr. Sci. 537 (2017) 128–139.